Chemical Physics Letters 498 (2010) 71–76

Contents lists available at ScienceDirect

Chemical Physics Letters

journal homepage: www.elsevier.com/locate/cplett

Ultrafast relaxation dynamics of photoexcitations in poly(3-hexylthiophene) for the determination of the defect concentration

Yu Hsien Lee [a,*], Atsushi Yabushita [a], Chain Shu Hsu [b], Sheng Hsiung Yang [c], Izumi Iwakura [d], Chih Wei Luo [a], Kaung Hsiung Wu [a], Takayoshi Kobayashi [a,e,f,g]

[a] Department of Electrophysics, National Chiao-Tung University, Hsinchu 300, Taiwan
[b] Department of Applied Chemistry, National Chiao-Tung University, Hsinchu 300, Taiwan
[c] Institute of Lighting and Energy Photonics, National Chiao-Tung University, Hsinchu 300, Taiwan
[d] Innovative Use of Light and Materials/Life, PREST, JST, 4-1-8 Honcho, Kawaguchi, Saitama 332-0012, Japan
[e] Department of Applied Physics and Chemistry and Institute for Laser Science, University of Electro-Communications, 1-5-1 Chofugaoka, Chofu, Tokyo 182-8585, Japan
[f] ICORP, JST, 4-1-8 Honcho, Kawaguchi, Saitama 332-0012, Japan
[g] Institute of Laser Engineering, Osaka University, 2-6 Yamada-oka, Suita, Osaka 565-0971, Japan

ARTICLE INFO

Article history:
Received 28 June 2010
In final form 17 August 2010
Available online 20 August 2010

ABSTRACT

Ultrafast pump–probe spectroscopy of poly(3-hexylthiophene) (P3HT) films was performed using a 9-fs laser and a broadband lock-in detection system. The fast geometrical relaxation (GR) time was attributed to the transition from a free exciton (FE) to form a bound polaron pair (BPP), and the time constant was estimated to be $\tau_{GR} = 90 \pm 2$ fs. The relaxation time constant of BPP was determined as $\tau_{BPP} = 710 \pm 40$ fs. The measurement of pump-power dependence enabled us to distinguish the defect trapping process of BPPs from other parallel decay processes and to determine the defect concentration of a P3HT thin film.

1. Introduction

Conjugated polymers have been studied extensively because of their characteristic properties, including plasticity and semiconductivity, that make them attractive for use in large-area devices for electro-optical and optoelectronic applications [1–8]. For instance, a considerable progress has been made in developing electroluminescent devices based on poly(arylenevinylene) [9,10] for an optoelectronic application, and organic solar cells that use conjugated-polymer-based compounds have recently been studied widely as a potential low-cost replacement for conventional silicon photovoltaics. Polymer-based solar cells have many advantages over conventional ones, including low toxicity, adjustable electronic and mechanical properties, and ease of fabrication. The energy conversion efficiency of a solar cell based on a bulk heterojunction consisting of a polymer donor of regioregular poly(3-hexylthiophene) (P3HT) and an acceptor of [6,6]-phenyl-C61-butyric acid methyl ester was reported to be 4.4% [11]. The dynamics of charge carriers contribution in P3HT was recently studied by Ellingson et al. [12] using THz pulses to probe the picosecond relaxation of P3HT, and the basic scheme of interchain transfer was also illustrated on the basis of previous works [13–15] with the formation and relaxation of bound polaron pairs. However, ultrafast formation and relaxation of BPP could not be time-resolved by the THz system due to the limited time-resolution of their measurement.

In the present study, we have studied the ultrafast dynamics of P3HT using a sub-10-fs visible laser pulse. The ultrafast time-resolution has enabled us to determine the time constants of 90 ± 2 and 710 ± 40 fs, which correspond to the formation and relaxation, respectively, of a bound polaron pair (BPP). Defect concentration on P3HT has also been estimated by observation of the pump intensity dependence of the signal.

2. Experiment

2.1. Non-collinear optical parametric amplifier

We have constructed a non-collinear optical parametric amplifier (NOPA) to generate visible laser pulses, whose spectral width is sufficiently broad to support sub-10 fs visible pulses useful for ultrafast time-resolved spectroscopy [16–18]. The smooth spectral shape of the NOPA output is suitable for time-resolved spectral measurements. A regenerative chirped pulse amplifier (Legend-USP-HE; Coherent) seeded with a Ti:sapphire laser oscillator (Micra 10; Coherent) is used to pump and seed the NOPA. The amplifier generates 40-fs pulses with a central wavelength of

* Corresponding author. Fax: +886 3 572 5230.
E-mail addresses: raymond.ep95g@nctu.edu.tw (Y.H. Lee), yabushita@mail.nctu.edu.tw (A. Yabushita).

0009-2614/$ - see front matter © 2010 Elsevier B.V. All rights reserved.
doi:10.1016/j.cplett.2010.08.036

800 nm, a repetition rate of 5 kHz, and an average power of 2.5 W. The beam from the regenerative amplifier is split into two beams by a beam sampler. One beam of 800 mW is used to generate a second harmonic of 400 nm to pump the NOPA. The other beam of 2.5 mW is focused on a sapphire plate to induce self-phase modulation to generate white light, which is used as the seed beam of the NOPA. The NOPA generates a broad visible spectrum extending from 520 to 700 nm with a nearly constant phase (see Fig. 1). A beam splitter splits the visible laser pulse into pump and probe beams. The intensities of these beams are adjusted using a variable neutral density filter, and the ratio of the pump to the probe intensities is set to be about four for the weakest excitation. The duration of the broadband visible laser pulse is compressed to 9 fs using a pulse compression system, which consists of a diffraction-grating telescopic dispersion line, specially designed multilayer dielectric chirped mirrors, and a computer-controlled flexible mirror. The probe pulse is dispersed by a polychromator (SP2300i; Princeton Instruments) into a 128-branch fiber bundle, whose other end is separated into 128 fiber branches and connected to avalanche photodiodes (APDs). Therefore, the time-resolved transmittance differences ΔT at 128 probe wavelengths are simultaneously detected at the APDs. The signals detected at the APDs are sent to a multichannel lock-in amplifier developed by our group to obtain a signal with a high signal-to-noise ratio.

2.2. Materials

Highly regioregular poly(3-hexylthiophene) (P3HT) (P200; Rieke Metals, Inc.) was purchased and used without further treatment. The sample had a HT(head-to-tail)-HT ratio of >98% and average molecular weight of 50,000. It was dissolved in 1,2-dichlorobenzene (15 mg/mL) stirring at 50 °C for 12 h to ensure complete dissolution. A P3HT thin film was formed by dip-coating on one surface of a glass substrate ($25 \times 25 \times 0.5\ mm^3$) to be used as a sample in this work. Figure 1 shows the stationary absorption spectrum of the formed P3HT film recorded using an ultraviolet–visible–near-infrared scanning spectrophotometer (UV-3101PC; Shimadzu). This figure also shows a photoluminescence spectrum measured by an ARC SpectraPro-150 luminescence spectrometer equipped with a deuterium lamp as an excitation light source. All measurements were performed at room temperature (295 ± 1 K).

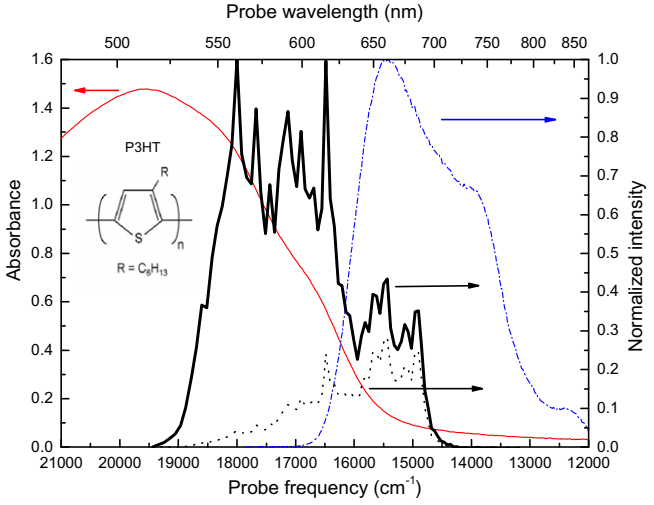

Figure 1. Stationary absorption spectrum (thin solid curve), laser spectrum (thick solid curve), transmittance spectrum (dotted curve), and fluorescence spectrum (dashed curve). The inset shows the molecular structure of P3HT.

3. Results and discussion

3.1. Time-resolved difference absorption spectra

Pump–probe measurements of P3HT films were performed to obtain time-resolved difference absorption spectra, $\Delta A(\lambda, t)$, in the wavelength range 530–680 nm in 2.5 nm steps; the scanning delay time was varied from −350 to 1400 fs in 3.6 fs steps. Figure 2a shows the observed two-dimensional (2D) ΔA spectrum, and Figure. 2b shows ΔA traces at eight probe wavelengths. The time traces contain an exponential decay reflecting electronic dynamics and oscillations reflecting vibration dynamics. We have performed exponential fitting to elucidate the ultrafast dynamics of the P3HT after photoexcitation; see below.

The difference absorbance, ΔA, is negative at short wavelengths and becomes positive at wavelengths longer than ~610 nm. The positive ΔA signal is assigned to induced absorption in transitions from the first electronic excited state to higher states. Stimulated emission from the excited state and photobleaching due to ground-state (GS) depletion could be the origins of the negative ΔA signal. The photobleaching has a much longer lifetime than the stimulated emission because stimulated emission occurs only from the excited singlet exciton state, whereas photobleaching occurs until the GS has been fully repopulated. Figure 2c shows the time-resolved absorbance change spectra averaged for 100 fs, which clearly indicates the existence of ultrafast decay in the spectral region shorter than 610 nm.

3.2. Estimation of time constants

It has been shown that photo-excited P3HT proceeds as follows [12]:

$$\mathrm{GS} \xrightarrow{h\nu} \mathrm{FE} \xrightarrow{\text{ultrafast}} \mathrm{BPP} \left\{ \begin{array}{c} \xrightarrow{\text{Recombination}} \\ \rightarrow \text{ Trapped-BPP } \rightarrow \\ \rightarrow \text{ Separated-Polaron } \rightarrow \end{array} \right\} \mathrm{GS} \qquad (1)$$

Here, FE is a free exciton, which undergoes a fast geometrical relaxation to form a BPP (equivalent to a self-trapped exciton). This generated BPP then relaxes to the GS via the three parallel processes of 'recombination', 'trapping by defect states', and 'dissociation into a positive carrier and a negative carrier (polarons)'. From the stationary absorption spectrum of the sample and the laser spectrum shown in Figure 1a, we estimated how many photons of a single laser pulse were absorbed by the P3HT sample, which is equal to the number of FEs formed by photoexcitation. When the pump power was 10.8 nJ, the FE density was calculated to be $1.8 \times 10^{19}\ cm^{-3}$. Using this FE density and the reported rate constant γ for exciton–exciton annihilation (EEA) in P3HT ($4.0 \times 10^{-9}\ cm^3\ s^{-1}$) [19], the mean flight time before EEA was estimated to be 14 ps, which is considerably longer than the measured delay time region of 1.5 ps. Therefore, the effect of EEA on the formation dynamics of BPPs from FEs was not considered here.

To determine the time constants of the above processes, the real-time traces of $\Delta A(\lambda, t)$ in the time region between 60 and 1400 fs were fitted with the sum of two exponential functions and a constant term. Two time constants, t_1 and t_2, determined by the fitting are shown in Figure 3a. In the longer wavelength region (from 620 to 680 nm), the ultrafast decay of ΔA is not prominent in comparison with that at wavelengths shorter than 620 nm, which is why the time constants could not be determined by the fitting in the longer wavelength region of Figure 3a. Global fitting was performed for the observed time-resolved 2D-ΔA trace to determine the time constants precisely (see Fig. 3b). The mean-square errors were calculated by varying the lifetimes in a stepwise

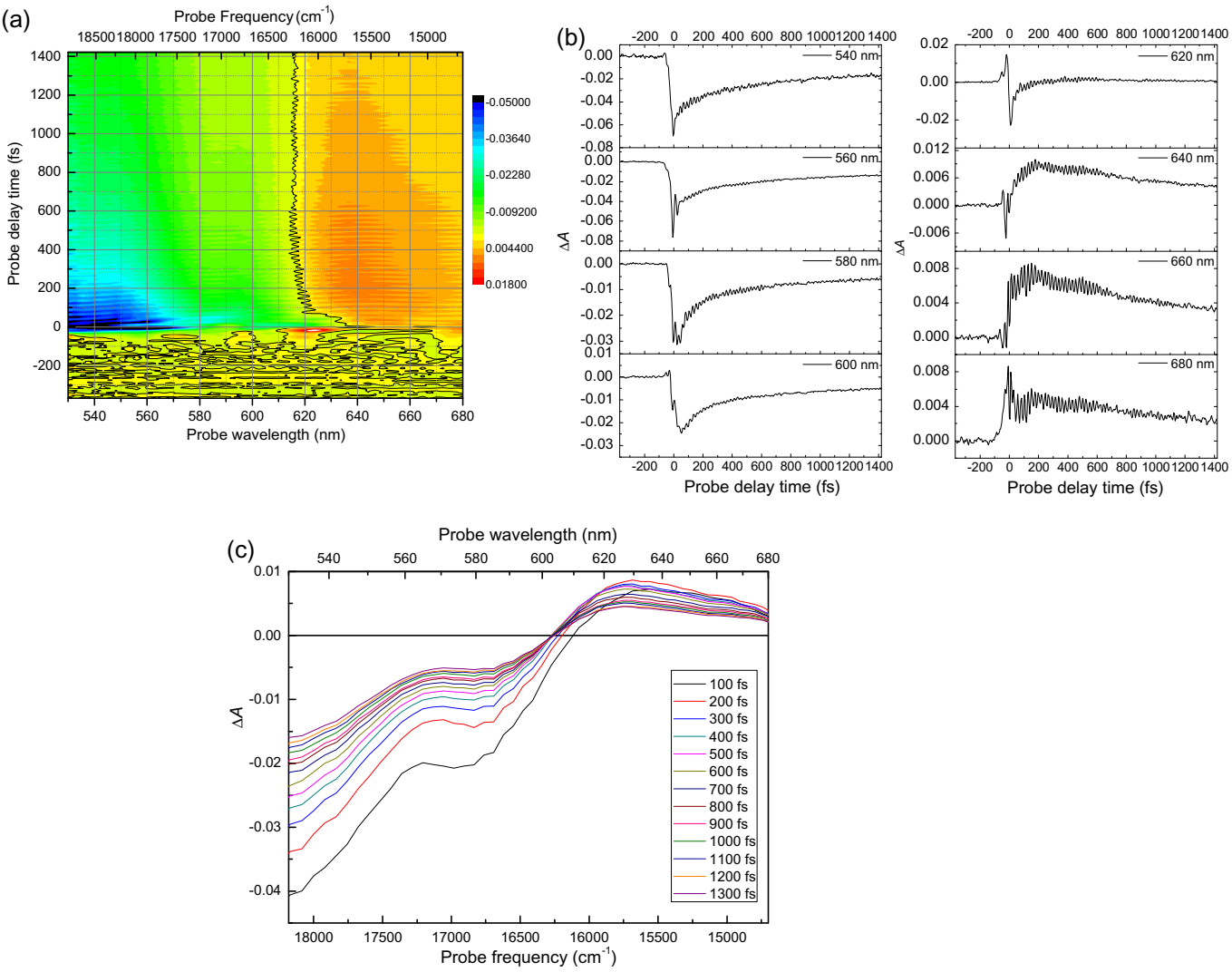

Figure 2. (a) Two-dimensional display of the time dependence of the absorbance changes (probe photon energy versus probe delay time).The value of ΔA is shown by a pseudocolor, and the curve represents the probe photon energy where $\Delta A = 0$. (b) Pump–probe delay time dependence of the difference absorbance probed at eight different wavelengths. (c) Time-resolved ΔA spectra averaged over 100 fs.

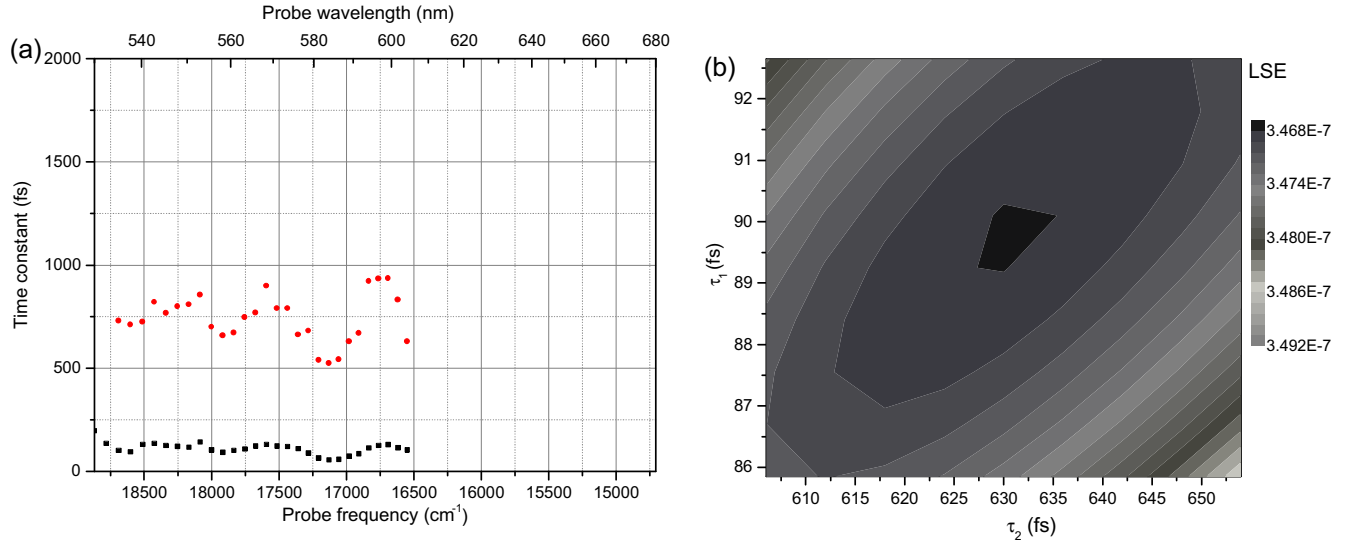

Figure 3. Time constants obtained by a calculation using a two-exponential fit performed for ΔA traces in (a) short delay region (from −0.35 to 1.4 ps) and (b) global fitting results for ΔA traces by the method of least-squares.

manner to determine the condition for the least-squares error. The results for three scans gave $t_1 = 90 \pm 2$ fs and $t_2 = 710 \pm 40$ fs.

The obtained values of t_1 and t_2 can be assigned to the formation and decay of a BPP, respectively, as were assigned to a self-trapped exciton in Refs. [13–15]. Self-trapped excitons only occur in one-dimensional systems being equivalent to bound polaron pairs (BPPs) [12,20,21]. A previous study estimated the formation time constant of a BPP to be shorter than 100 fs, but it was not time-resolved [14]. The t_1 constant of BP formation P, 90 ± 2 fs, has first been time-resolved in this work, as stated above.

3.3. Spectra of the intermediates

Using the obtained t_1 and t_2 constants, changes in the time-resolved absorption spectra, $\Delta A(\lambda, t)$, were fitted by a double exponential function,

$$\Delta A(\lambda, t) = b_1(\lambda)e^{-t/t_1} + b_2 e^{-t/t_2} + b_0(\lambda) \quad (t_1 < t_2) \tag{2}$$

in the ranges of 60–1400 fs and 550–600 nm applying the method of least-squares. The $b_0(\lambda)$, $b_1(\lambda)$, and $b_2(\lambda)$ coefficients obtained in the fitting can be used to calculate $b_{FE}(\lambda)$ and bBPP(λ), which represent the contribution from FE and BPP, respectively, as stated below.

Photo-excitation of P3HT generates FE, which makes a transition to BPP with t_{FE}. The BPP relaxes in three parallel processes: 'recombination', 'trapping', and 'dissociation'. The whole processes can be expressed by

$$\Delta A(\lambda, t) = b_{FE}(\lambda)e^{-t/t_{FE}} + b_{BPP}(\lambda)(1 - e^{-t/t_{FE}})e^{-t/t_{BPP}} + b_{RBPP}(\lambda) \times (1 - e^{-t/t_{FE}})(1 - e^{-t/t_{BPP}}) \tag{3}$$

where suffixes FE and BPP correspond to a free exciton and a bound polaron pair. The last term of RBPP stands for relaxed BPP made of trapped BPP and separated polaron, whose lifetimes are much longer than the time region studied in this work. For simplicity of calculation, a single time constant of t_{BPP} represents the contributions of three parallel decay processes of BPP, which are decomposed by studying pump-power dependence; see Section 3.5.

The time constants t_1 (90 ± 2 fs) and t_2 (710 ± 40 fs), assigned in Section 3.2 to the formation and decay of BPP, correspond to t_{FE} and t_{BPP} of Eq. (3). Therefore, Eq. (3) can be approximated by considering $\tau_{FE} \ll \tau_{BPP}$ as

$$\Delta A(\lambda, t) = b_{FE}(\lambda)e^{-t/t_{FE}} + b_{BPP}(\lambda)(e^{-t/t_{BPP}} - e^{-t/t_{FE}}) + b_{RBPP}(\lambda) \times (1 - e^{-t/t_{BPP}}) \tag{4}$$

Using Eqs. (2) and (4), we obtain

$$b_1(\lambda) = b_{FE}(\lambda) - b_{BPP}(\lambda) \tag{5}$$

$$b_2(\lambda) = b_{BPP}(\lambda) - b_{RBPP}(\lambda) \tag{6}$$

$$b_0(\lambda) = b_{RBPP}(\lambda) \tag{7}$$

These three equations give

$$b_{BPP}(\lambda) = b_2(\lambda) + b_0(\lambda) \tag{8}$$

$$b_{FE}(\lambda) = b_1(\lambda) + b_2(\lambda) + b_0(\lambda) \tag{9}$$

Using the two relations, $b_{FE}(\lambda)$ and $b_{BPP}(\lambda)$ can be calculated from $b_0(\lambda)$, $b_1(\lambda)$ and $b_2(\lambda)$ obtained in the double exponential fit. The calculated $b_{FE}(\lambda)$ and $b_{BPP}(\lambda)$ are shown in Figure 4a.

3.4. Defect concentration studied by pump-power dependence

The b_{FE} term reflects the transition from a FE to a BPP [12,20]. Since b_{FE} is negative showing a spectral structure similar to that of a stationary absorption spectrum in the range of 530–630 nm, it can be ascribed to photobleaching as a result of GS depletion. The spectrum of the second component b_{BPP}, on the other hand, corresponds to the spectrum of BPP state, which follows relaxation induced by 'recombination returning to the GS', 'trapping by defects', and 'dissociation into a positive carrier and a negative carrier (polarons)' [12]. The spectral structure of b_{BPP} in the region of the probe wavelength shorter than 610 nm is similar to that of b_{FE}, showing the contribution of photobleaching. Subtraction of b_{FE} (contribution of photobleaching) from b_{BPP} leads to a positive ΔA component, as shown in Figure 4a, which reflects the induced absorption spectrum of BPP. The last term of Eq. (4) is a long-lifetime component; being beyond the range of our time measurement, it is attributed to the decay of BPPs including the delocalization of charge carriers along the polymer chain [12].

As discussed above, b_{BPP} is composed of three parallel relaxation components of recombination ($b_{BPP,REC}$), defect trapping ($b_{BPP,TRP}$), and dissociation ($b_{BPP,DIS}$). The $b_{BPP,TRP}$ component is likely to be independent of the pump intensity when the pump intensity is high enough to cause the trapping process to saturate due to the finite number of traps. In contrast, $b_{BPP,REC}$ and $b_{BPP,DIS}$ are proportional to the pump intensity, since no saturation effects are expected in the recombination and dissociation processes. Therefore, when the $b_{BPP,TRP}$ absorption is saturated resulting in homogeneous broadening, the coefficient of the second component is given by

$$b_{BPP}(I) = b_{BPP,\,TRP} + (b_{BPP,\,REC} + b_{BPP,\,DIS}) = C_1 I(1 + I/I_S)^{-1} + C_2 I \tag{10}$$

where I and I_s are the pump intensity and the saturation pump intensity, respectively. C_1 and C_2 are the fitting parameters. Therefore, $b_{BPP,TRP}$ can be separated from $b_{BPP,REC} + b_{BPP,DIS}$ if we perform pump–probe measurements varying the pump intensity.

Figure 4b shows b_{BPP} obtained by varying the pump intensity. The pump pulse energy was set to 3.2, 4.4, 6.4, 8.4, and 10.8 nJ, while the probe pulse energy was fixed at 0.9 nJ. We investigated the dependence of the area of the b_{BPP} spectrum between 550 and 600 nm on the pump power, and we estimated the ratio of C_1:C_2. In Figure 4c, the pump-power dependence of b_{BPP} integrated over the spectral range is plotted with a fitting curve fitted by the function shown in Eq. (10). From the fitting result, I_s is estimated to be 7 ± 3 nJ and C_1:C_2 was calculated to be 0.46 ± 0.02:0.53 ± 0.05.

The number of trapped BPPs (n_{TRP}) in P3HT can be determined by

$$n_{TRP} = P(C_1 I(1 + I/I_S)^{-1})/(C_1 I(1 + I/I_S)^{-1} C_2 I) \tag{11}$$

where P is the number of absorbed photons and Figure 4d shows the observed pump-power dependence of the number of the trapped BPPs. The limit of the number of trapped BPPs as I approaches infinity gives the number of the defect sites on P3HT, and the defect concentration is estimated to be 1.2×10^{19} cm^{-3}.

A previous study found that a lamellar structure is formed on P3HT thin films [22], resulting in a lower relaxation energy for interchain charge transfer than that for one-dimensional chains. When all the BPPs (i.e., self-trapped excitons) have undergone interchain transfer, they have the possibility to be trapped by the defect sites. We have estimated the volume of a single chain of P3HT to be 3.95×10^{-20} cm^3 by a Monte Carlo method. Based on the defect concentration and the volume of P3HT chains, we estimate that on average about two defect sites are present in the volume occupied by three P3HT chains in this sample. This leads to the conclusion that the generated BPPs are not trapped at the end of the main chain but are reflected back from the ends.

3.5. Decomposition of parallel decay rates of BPP

The time constants of defect trapping, recombination, and dissociation of BPP are estimated as follows. The ultrafast growth

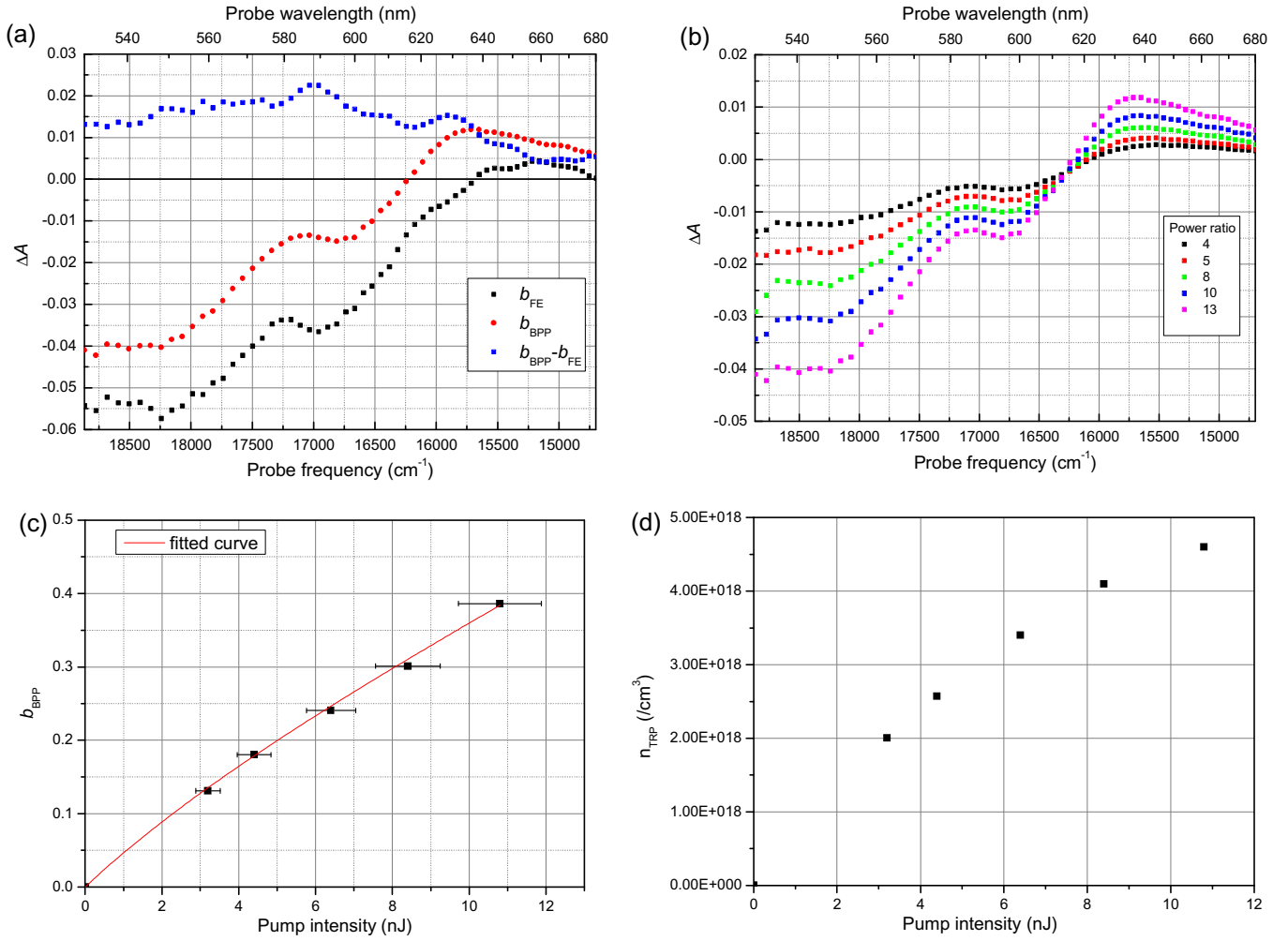

Figure 4. (a) Difference absorption spectra corresponding to ultrafast decaying free-excitons minus the ground-state (b_{FE}), sub-picosecond decaying bound polaron pairs minus the ground-state (b_{BPP}), and the difference between b_{BPP} and b_{FE}, which reflects induced absorption of bound polaron pairs ($b_{BPP} - b_{FE}$). (b) Pump intensity dependence of b_{BPP}. (c) Fitting curve for b_{BPP} observed at different pump intensities. (d) Density of trapped BPP at different pump intensity.

and fast relaxation are expressed by τ_{GR} and τ_{BPP} respectively assuming that they obey the following relationships:

$$\tau_{GR} = (\kappa_{FE\rightarrow BPP})^{-1} \tag{12}$$

$$\tau_{BPP} = (\kappa_{TRP} + \kappa_{DIS} + \kappa_{REC})^{-1} \tag{13}$$

where κ_i (i = FE → BPP, TRP, DIS, REC) represents the rate constants for formation, defect trapping, dissociation, and recombination of BPP.

The ratios between the parallel decay processes of BPP are given as

$$\eta_i = \kappa_i(\kappa_{TRP} + \kappa_{DIS} + \kappa_{REC})^{-1} \tag{14}$$

where i is TRP, DIS, REC. From the above study of pump-power dependence, we can determine that

$$\kappa_{TRP} = \eta_{TRP}(\tau_{BPP})^{-1} \quad \text{and} \tag{15}$$

$$\kappa_{DIS} + \kappa_{REC} = (\eta_{DIS} + \eta_{REC})(\tau_{BPP})^{-1} = (1 - \eta_{TRP})(\tau_{BPP})^{-1} \tag{16}$$

Under the highest excitation (10.8 nJ), the ratio between TRP and REC + DIS is estimated to be 1:3 by Eq. (10) showing that the 710 ± 40 fs decay of BPPs consists of a 2.8 ± 0.1 ps relaxation caused by defect trapping and a 0.95 ± 0.05 ps relaxation caused by recombination and dissociation into positive and negative carriers (polarons). Therefore, the reactions of P3HT after photoexcitation in the highest excitation case can be summarized as follows:

$$\mathrm{GS} \underset{10.8\ \mathrm{nJ}}{\overset{h\nu}{\rightarrow}} \mathrm{FE} \overset{90\pm2\ \mathrm{fs}}{\rightarrow} \mathrm{BPP} \left\{ \begin{array}{l} \overset{\text{Recombination}}{\rightarrow} \\ \overset{2.8\pm0.1\ \mathrm{ps}}{\rightarrow}\ \text{Trapped-BPP} \rightarrow \\ \rightarrow\ \text{Separated-Polaron} \rightarrow \end{array} \right\} \mathrm{GS} \tag{17}$$

4. Conclusions

A pump–probe measurement of a P3HT thin film has been performed using 9-fs laser pulses. Due to the extremely high temporal resolution of these measurements, the time constant for the formation of BPPs (which had previously been known to be ~100 fs) has now been measured with higher accuracy to be 90 ± 2 fs and the time constant for the BPP decay to be 710 ± 40 fs (see Fig. 3). The traces of the ultrafast time-resolved absorbance change (ΔA) have been measured simultaneously at 128 probe wavelengths over the broadband visible spectral region. The observed 2D-ΔA data is decomposed by the LSE analysis to obtain the ΔA spectrum related to FE and BPP. The pump-power dependence is used to determine the number of trapped BPPs, whose maximum value reflects the number of the defect sites on P3HT. The concentration of the

defects (which trap BPPs) in the P3HT film is thus found to be $1.2 \times 10^{19}\,cm^{-3}$. Based on this estimation, we conclude that two out of the three main chains have a defect and that the chain ends do not trap BPPs.

Acknowledgements

This work has been supported in part by a grant to A.Y. from the National Science Council, ROC (NSC 98-2112-M-009-001-MY3) by the 21st Century COE Program on 'Coherent Optical Science', and by a grant from the Ministry of Education (MOE) in Taiwan under the ATU Program at National Chiao Tung University. A part of this work has been performed under the joint research project of the Laser Engineering, Osaka University under contract subject B1-27.

References

[1] T. Blythe, D. Bloor, Electrical Properties of Polymers, Cambridge University Press, Cambridge, 2002.
[2] C. Brabec, V. Dyakonov, J. Parisi, N.S. Sariciftci, Organic Photovoltaics: Concepts and Realization, Springer, Berlin, 2003.
[3] R.H. Friend et al., Nature 397 (1999) 121.
[4] N. Tessler, G.J. Denton, R.H. Friend, Nature 382 (1996) 695.
[5] G. Hadziioannou, P.F.V. Hutten, Semiconducting Polymers, Wiley-VCH, Weinheim, 2000.
[6] A. Kohler et al., Nature 392 (1998) 903.
[7] B.J. Schwartz, Annu. Rev. Phys. Chem. 54 (2003) 141.
[8] E. Hendry, J.M. Schins, L.P. Candeias, L.D.A. Siebbeles, M. Bonn, Phys. Rev. Lett. 92 (2004) 196601.
[9] J.M. Kang, M.J. Park, S.K. Kim, C. Lee, S.H. Jin, D.H. Hwang, Curr. Appl. Phys. 6 (2006) 756.
[10] D.H. Hwang et al., Curr. Appl. Phys. 9 (2009) 441.
[11] G. Li, V. Shrotriya, J.S. Huang, Y. Yao, T. Moriaty, K. Emery, Y. Yang, Nat. Mater. 4 (2005) 864.
[12] X. Ai, M.C. Beard, K.P. Knutsen, S.E. Shaheen, G. Rumbles, R.J. Ellingson, J. Phys. Chem. B 110 (2006) 25462.
[13] T. Kobayashi, M. Yoshizawa, U. Stamm, M. Taiji, M. Hasegawa, J. Opt. Soc. Am. B 7 (8) (1990) 1558.
[14] T. Kobayashi, Syn. Met. 71 (1995) 1663.
[15] A. Matsuse, S. Takeuchi, K. Yoshino, T. Kobayashi, Chem. Phys. Lett. 288 (1998) 165.
[16] A. Shirakawa, I. Sakane, T. Kobayashi, Opt. Lett. 23 (1998) 1292.
[17] A. Shirakawa, I. Sakane, M. Takasaka, T. Kobayashi, Appl. Phys. Lett. 74 (16) (1999) 2268.
[18] A. Baltuska, T. Fuji, T. Kobayashi, Opt. Lett. 27 (2002) 306.
[19] P.E. Shaw, A. Ruseckas, I.D.W. Samuel, Adv. Mater. 20 (2008) 3516.
[20] A. Ruseckas, M. Theander, M.R. Andersson, M. Svensson, M. Prato, O. Inganäs, V. Sundström, Chem. Phys. Lett. 322 (2000) 136.
[21] B. Kraabel, D. McBranch, N.S. Sariciftci, D. Moses, A.J. Heeger, Phys. Rev. B 50 (1994) 18543.
[22] H. Sirringhaus et al., Nature 401 (1999) 685.